Reactive transport of Sr at two laboratory-scale columns: experiments and modeling

Christelle Latrille, Aubéry Wissocq, Catherine Beaucaire, Olivier Bildstein

To cite this version:

Christelle Latrille, Aubéry Wissocq, Catherine Beaucaire, Olivier Bildstein. Reactive transport of Sr at two laboratory-scale columns: experiments and modeling. Journal of Contaminant Hydrology, 2021, pp.103850. 10.1016/j.jconhyd.2021.103850 . cea-03540707

Reactive transport of strontium in two laboratory-scale columns: experiments and modelling

Christelle Latrille[a*], Aubéry Wissocq[a,b], Catherine Beaucaire[a,b], Olivier Bildstein[c]

[a] Université Paris-Saclay, CEA, Service d'Etude du Comportement des Radionucléides, 91191, Gif-sur-Yvette, France

[b]LAMBE, CEA, CNRS, Université Paris-Saclay, 91000, Evry, France

[c] CEA-DES-IRESNE-DTN Cadarache F-13108 Saint-Paul-Lez-Durance, France

Corresponding author. Tel.: +33-(0)169-083-424; fax: +33-(0)169-083-242.
E-mail address: christelle.latrille@cea.fr

Keywords: illite; smectite; strontium; reactive transport; ion exchange model

Abstract

To support the environmental monitoring of nuclear sites, reactive transport models used to predict the migration of contaminants such as strontium-90 (^{90}Sr) in soils, sediments and aquifers are developed, continuously tested and improved. This study aims at assessing the adequacy of the multi-site ion exchanger model (MSIE) based on a component "additivity approach" and coupled to the advection-dispersion equation (ADE) to simulate Sr transport in a clayey sandstone and a Bt soil horizon. We have also compared the performance of the modelling approach with simulation results obtained by considering a K_d approach (constant K_d). Transport experiments were performed in centimetre- and decimetre-scale columns in order to test the model sensitivities to the mineral abundance and the specificities of their reactive parameters. Non-reactive transport experiments with conservative tracers allowed us to determine the transport parameters, such as porosity and dispersivity. In this paper, we have compared the Sr transport simulation results with Sr experimental breakthrough curves acquired at various flow velocities. The simulations results show that the K_d approach can reproduce experimental data in the case of the clayey sandstone when a certain amount of uncertainty is accepted, whereas the additivity approach better fits the Sr reactive transport in both columns (especially the maximum value) without it being necessary to adjust the parameters. These results advocate for more complex retention models than K_d to better understand and improve the robustness of Sr transport predictions. The clay content, the relative abundance of illite and smectite, and the clay mineral specificity, are all sensitive parameters when it comes to defining the reactive system involved in Sr transport simulation. The results highlight the influence of illite in the spreading of the Sr breakthrough curve, especially through its low-capacity and high-selectivity site. This implies having access to a robust and extensive set of retention parameters acquired on reference minerals. In this study, the results obtained for the clayey sandstone confirm the robustness of our selected parameters when clay minerals have similar reactivity levels as the reference minerals. This set of parameters appears more limited in the case of the Bt soil containing weathered or evolved minerals. The choice of modelling approach is therefore crucial for accurately modelling and predicting Sr transport behaviour in porous media, as is the representativeness of the minerals in the database.

1. Introduction

^{90}Sr is a product of uranium and plutonium fission generated in nuclear reactors and is one of the most abundant radioisotopes released into the environment because of weapons testing and nuclear accidents (Kashparov *et al.* 2003). ^{90}Sr (29 years half-life) is highly soluble and its sorption is strongly affected by competition with major cations in solution, i.e. with Ca and Mg. Moreover, it generally does not remain on the soil surface like Cs (Berns *et al.*, 2018), which facilitates its migration to greater depths. To support the environmental monitoring of nuclear sites, reactive transport models are being developed to simulate the migration of contaminants such as ^{90}Sr in soils, sediments and aquifers, the key requirement being a robust predictive performance.

Reactive transport processes, i.e. advection, dispersion and diffusion coupled with chemical reactions involving precipitation, dissolution or adsorption-desorption, generally control contaminant migration in natural environments. They result in retarded migration, often expressed by a delay with respect to water tracers or by tails in the breakthrough curve (Liu *et al.*, 2017). The time dependence of reactive transport requires examining both transport processes and reactivity formalisms used in the modelling approaches. The sorption of contaminants has been modelled using simple, empirical retention models such as linear (constant distribution coefficient K_d), Langmuir or Freundlich sorption isotherms (Bachhuber *et al.*, 1982; Hölttä *et al.*, 1997, Cui *et al.*, 1998; Fesch *et al.*, 1998; Palagyi and Stamberg, 2010). However, such models provide specific and contextual parameters determined in precise physicochemical conditions and therefore often fail to be predictive. For instance, Szenknect *et al.* (2008) simulated Sr transport through a sandy soil column using a constant K_d. These authors highlighted the fact that Sr reactive transport deviates from classical reactive transport including a retardation factor, although Sr sorption was described as instantaneous, reversible and with a linear reaction at trace concentration (Szenknect *et al.* 2005, Wissocq *et al.*, 2018). Moreover, to simulate Sr transport in field experiments through aeolian sand sampled from the Chernobyl site, Bugai *et al.* (2012) found K_d values to be the most sensitive parameter in the model. In this study, the K_d values obtained by laboratory batch tests (Szenknect *et al.*, 2005) had to be adjusted to match the simulation outcomes with the observed data. The mismatch was attributed to geochemical disturbances involving changes in the competing cation (i.e. Ca) concentration in solution. Bugai *et al.* (2020) cautioned against the concomitance of the adsorption/desorption reaction with other chemical processes in the natural environment. Modelling on an aquifer scale can then be distorted by taking into account K_d values measured in the laboratory that are not representative of the processes involved.

Another approach consists in coupling transport and thermodynamic retention models to account for varying physicochemical conditions in the media. Ion-exchange models have often been retained for multi-components materials (Vallochi *et al.*, 1981a and b; Schweich and Sardin, 1981; Appelo, 1994; Vulava *et al.*, 2000; Steefel *et al.*, 2003; Lichtner *et al.*, 2004; Missana *et al.*, 2008; Tournassat *et al.*, 2013). Despite better consideration of the chemical reactions by these retention models, some authors were required to adjust the sorption parameters obtained in batch experiments for trace elements (static conditions) in order to reproduce reactive transport data (Steefel *et al.*, 2003; Szenknect *et al.*, 2005), therefore diminishing the predictability of these reactive transport models. To apply the retention parameters acquired in dispersed multicomponent media (i.e. batch experiments) to compacted media (i.e. column or field experiment), it must be assumed that the entire solid is in contact with solution so that all the sorption sites are called into play in the reactive process.

Among the tested approaches, the generalised composite approach consists in considering only one ion-exchange site-bearing component to reflect the material’s reactivity. However, it was previously shown that the strongest affinity for trace elements (i.e. Sr, Zn, Tl, Cs…) on clay minerals is associated to specific sorption sites (Poinssot *et al.*, 1999, Missana *et al.*, 2008, 2014, Altmann *et al.*, 2015, Wissocq *et al.*, 2017, Martin *et al.*, 2018, Latrille *et al.*, 2019, Tournassat *et al.*, 2013), which are usually not differentiated in such a retention approach. By using a generalised composite approach, Voegelin *et al.* (2000) and Vulava *et al.* (2002) were able to use the same dataset in static and dynamic conditions to reproduce the transport of major elements (Ca, Mg and Na) and Sr in trace form (Szenknect *et al.*, 2008). However, this approach is restricted to a specific context, which constrains its extrapolation to other multi-component materials and extended environmental conditions. Vulava *et al.* (2002) compared various exchange models and evidenced a significant improvement was gained with a multi-site cation exchange model to predict the transport behaviour of the major cations. Lu *et* *al.* (2014) also made this assessment and used such a model to cover a large range of chemical conditions without any adjustable parameters. Another approach is to resort to a multi-site ion exchanger model using a component additivity approach, which takes into account the retention of contaminants on pure mineral phases (Peynet, 2003) so as to predict the retention of a multi-component assemblage. Wissocq *et al.* (2018) demonstrated its efficiency by predicting Sr retention on a clayey sandstone without adjusting any of the parameters. Coupled with a transport model, this multi-site ion exchanger model has proved efficient in predicting the reactive transport of key elements (Na and Ca) in a pure phase and a soil using the same dataset in static and dynamic conditions (Tertre *et al.*, 2013; Lu *et al.*, 2014).

This study aims at assessing the adequacy of the multi-site ion exchanger model coupled with a transport model to simulate Sr transport in natural materials. In this framework, the material retention properties were taken into account by the additivity approach based on their mineralogical compositions in reactive phases. Furthermore, the performance of our modelling approach was also compared against simulation results obtained by considering a K_d approach, which is commonly used in environmental impact calculations. The sensitivity of the additivity approach was tested by comparing Sr transport simulations carried out using data acquired by Latrille *et al.* (2017) with data from new experiments in a column filled with a clayey sandstone (on the scale of the centimetre and decimetre). For this purpose, the influence of i) the mineral abundance and ii) the reactive parameters of these minerals, on the simulation results was evaluated. To do this, we used breakthrough curves established on the basis of two different length scales columns. In order to explore the scope of this approach, a Bt soil horizon (Latrille *et al.*, 2017, Lu *et al.*, 2014) was chosen with relative abundances of illite and smectite differing to those found in the clayey sandstone. The simulations were performed by coupling the advection-dispersion equation (ADE) with the multi-site ion exchanger model (MSIE) using both the sorption property database for illite and smectite recently established in batch experiments by Wissocq *et al.* (2018), and the specific experimental input parameters relative to each operating condition.

2. Materials and methods

2.1. Materials

The first material was a clayey sandstone (CS), which has already been described in detail by Wissocq *et al.* (2018). This clayey material was sampled from a depth of 31 metres in the Miocene geological formation located at the Cadarache nuclear research centre (France). The rock sample was manually crushed, air dried and sieved at 300 µm and 200 µm. The crushed bulk material was used to fill the decimetre-scale column whereas a dried 300-200 µm fraction was selected for the centimetre-scale column. The < 25 µm fraction was isolated from the raw CS by dispersion in water followed by sieving to 25 µm. The mineralogical composition was determined by X-ray diffraction (XRD) on air-dried powder for the bulk material and on air-dried deposits and deposits saturated with ethylene glycol for the < 25 µm fraction. Identification of crystallised phases was performed using the ClayXR software (Bouchet, 1992) and NEWMOD© software (Reynolds, 1985) was used for quantification. The bulk material was mainly composed of quartz (75 wt%), clay minerals (20 wt%), carbonates (2.5 wt%) and iron oxides (2.5 wt%). The XRD mineralogical quantification of the < 25 µm fraction extracted from the raw material, revealed about 32 wt% of kaolinite, 20 wt% illite, 19 wt% smectite, 2 wt% chlorite, 17 wt% quartz and 10 wt% goethite, and no carbonates. Cation exchange capacity (CEC) measurements on raw material, 300-200 µm and < 25 µm fractions were performed by K^+/Cs^+ cation exchange at pH 9. The resulting average value were respectively 0.112 ± 0.006, 0.064 ± 0.020, 0.326 ± 0.020 eq/kg (Wissocq *et al.* (2017)). In our experimental chemical conditions (pH 6.5), goethite remained positively charged (Hayes and Leckie, 1987; Villalobos and Leckie, 2000) and was therefore considered as a non-reactive phase. Weighted by their relative abundance, chlorite and kaolinite contributed to the material exchange capacity at a level equivalent to the CEC measurement uncertainty (0.020 eq/kg, 6.3 % of material CEC). Consequently, smectite and illite were assumed to govern the sorption processes. The reactive phases were therefore estimated equivalent to 27.7 % of illite and 26.7 % of smectite in the < 25 µm fraction. Illite and smectite content in the raw soil and in the 300-200 µm fraction are calculated by weighting their amount in the < 25 µm fraction to the CEC of the corresponding material.

The second material investigated in this study was a Bt horizon of a Luvisol (Bt) previously described and studied by Lamy *et al.* (2006) and Lu *et al.* (2014). The grain size distribution of this sandy clay horizon was 70.7 wt% of sand, 8.9 wt% of silt and 20.4 wt% of clay, and it contained only 0.34 wt% of organic matter. The < 2 mm air-dried soil was sieved at 300 µm and 250 µm to extract the material used to fill the centimetre-scale column. The CEC was measured at 0.13 ± 0.01 eq/kg (Lu *et al.*, 2014) and this fraction contained 18 wt% of clay. The clay minerals identified by XRD were kaolinite, illite, and illite/smectite mixed layers. Clay minerals were quantified by modelling the X-ray diffraction pattern in both air-dried and ethylene-glycol-solvated states, acquired on the clay size-fraction with the Sybilla© software developed by Chevron™ (Aplin *et al.*, 2006). The assemblage consisted of discrete illite (2.3 %), mixed-layers illite/smectite with 56.2 % IS (40/60) and 5.1% IS (29/71), and discrete smectite (36.4 %). For the purpose of modelling, the mineralogical composition of the clay size-fraction was therefore assimilated to 26.2 % of illite and 73.8 % of smectite.

2.2 Solutions and analytical methods All chemicals used were at least of analytical grade. $CaCl_2$ (VWR Chemical) salt solutions and the Sr solutions were prepared with a $SrCl_2$ $6H_2O$ salt (99.995% trace metals basis, Sigma Aldrich) dissolved in Milli-Q water (Millipore®, 18.2 MΩ.cm^2). Chemical analyses were carried out by ionic chromatography (standards Chem-Lab) for Ca and by inductively coupled plasma mass spectrometry (ICP-MS) (Plasma CAL standards) for Sr. The measurement uncertainties were estimated at 2 %.

Non-reactive tracers chosen for these experiments were ^2H ($^2H/^1H = 2000$), Cl^- in a $CaCl_2$ solution and I^- in a CaI_2 solution (10^{-1} M). ^2H was mixed in a 10^{-2} M $CaCl_2$ solution. ^2H concentrations were analysed with a deuterium analyser (Los Gatos Research Liquid-Water Stable Isotope Analyser). Cl^- concentrations were measured by ionic chromatography. Cl^- and I^- concentrations were also directly measured using an on-line electrical conductivity cell in the centimetre- and decimetre-column devices.

The pH was measured using a combined glass pH electrode (Mettler Toledo) equipped with an Ag/AgCl reference electrode. The electrode was calibrated with buffer solutions at pH 4, 7 and 12.

2.3 Column transport experiments

2.3.1 Experimental set-ups

Column transport experiments were performed on a centimetre- and a decimetre-scale column. Both columns were placed in two adapted set-ups designed according to the same configuration shown in Figure 1 and SI-1 (Latrille *et al.*, 2017).

This configuration included an HPLC pump (Hitachi LaChrom Elite L-2130) which regulated the flow rate through the column. Two conductivity cells and pH electrodes (Amersham, Biosciences) were placed on-line, arranged on each side of the column. Finally, a fraction collector (Omnicoll®, Lamda) was used to receive and sequentially redistribute the outflowing solution in aliquots. Outflow tracer concentrations were then analysed by ion chromatography (Cl^-), electrical conductivity (CaI_2) and ICP-MS (Sr).

For the column experiments performed on a centimetre scale (SI-1), two glass chromatography columns (Omnifit®) were filled by successively adding the material (respectively CS material in column C1 and Bt material in column C3), compacted using a uniaxial press, to achieve a packed length of 7.1 cm and a diameter 1 cm. Table 1 summarises the details of the packed columns according to their geometric and physical features. The columns were saturated from the bottom with the deaerated 10^{-2} M $CaCl_2$ background solution and conditioned until equilibrium with this solution by flowing ca. 500 pore volumes (v_p) through column C1 and 200 v_p through column C3.

Column	C1	C2	C3
Material	CS 300-200 µm	Bulk CS	Bt 300-250 µm
Length (cm)	7.1	35	7.1
Diameter (cm)	1	5	1
Porosity	0.362	0.326	0.518
Pore volume (cm^3)	2.02	225	2.85
Bulk density[a] ($g.cm^{-3}$)	1.69	1.79	1.65

[a] bulk density based on the dry solid mass introduced on filled volume ratio

Table 1: Geometric and physical properties of the three columns

At decimetre scale (Figure 1), the column experiments were performed by using the BEETI experimental device (Latrille and Cartalade, 2010). It was composed of a vertical polycarbonate column filled with bulk CS compacted in a uniaxial press, a controlled hydraulic circuit that enforced tracer migration, and a dichromatic X-ray spectrometer (DXS). Based on X-ray attenuation measurements, porous material properties (porosity, bulk density, water content and clay proportion) and resident concentrations of attenuating tracers can be quantified down the entire column (Figure 1). These measurements were used to evaluate the solid homogeneity and the water content in the compacted column. Moreover, depending on the calibration process, the clay proportion distribution along the column can also be estimated. Resident concentration profiles of the inert tracer CaI_2 were measured at eight specific locations down the column in order to determine the variability of dispersivity.

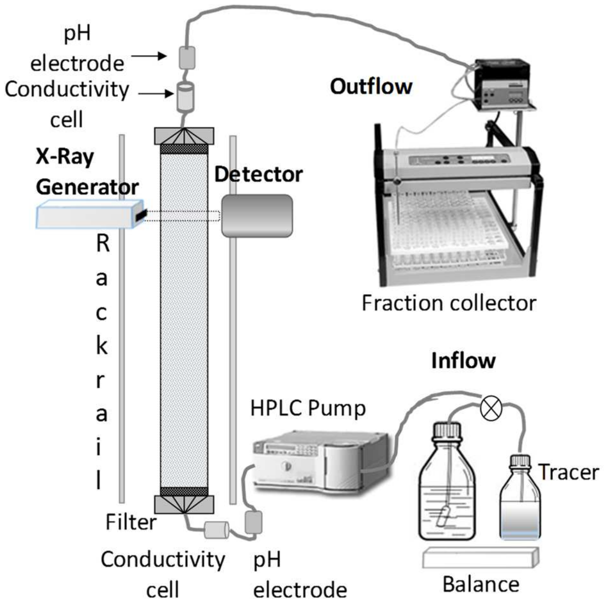

Figure 1. BEETI experimental set-up for transport column experiments at decimetre scale

X-ray attenuation measurements were performed using a dichromatic X-ray spectrometer (DXS) which combined an X-ray generator and a NaI detector (Latrille and Cartalade, 2010; Latrille and Néel, 2013). The X-ray beam was emitted in two energy ranges 20 – 40 keV and 50 – 75 keV. After crossing the column filled with the porous material, the NaI detector measured the beam count-rate. The source and detector were simultaneously moved up and down the column by a controlled rack rail

(Figure 1), and kept at specified locations ($0 < x < 32$ cm) during a set counting time (80 s). The X-ray count-rate measured by the detector depended on the thickness and the type of the phases encountered on the transmission path (fluid, bulk CS or clay and inert CaI_2 tracer), as well as on the counting time. At each longitudinal location x on the column, the thickness of each phase was determined by solving the Beer-Lambert's law (Eq. 1):

$$I = I_0 exp(-\sum_i \mu_i \rho_i z_i) \qquad \text{(Eq. 1)}$$

Where, I_0 is the count-rate emitted by the source; I is the count-rate detected per unit time for a given X-ray energy range and transmitted throughout a column slice (5 mm x 20 mm); index i represents each phase contained in the medium (clay or bulk CS, background solution, solute tracer); μ_i (m^2/kg) is the mass attenuation coefficient, which depends on the phase composition and on the X-ray energy; ρ_i (kg/m^3) is the density, and z_i (m) is the thickness of the phase. The mass attenuation coefficients of clay, bulk CS, background solution (10^{-2} M $CaCl_2$) and tracer solution (CaI_2) were therefore determined in this configuration using specific standards defined on the basis of the component chemical composition. Calibration sequences were performed prior to experiments, as detailed in Latrille and Néel (2013), to acquire the bulk CS standard and the clay standard. A specific calibration allowed us to then determine the clay mineral attenuation by accounting for its chemical composition acquired on the clay fraction extracted from bulk material. The clay mineral attenuation is distinguished from that of sand in order to calculate the relative proportion of clay at each x position along the column. The resident tracer concentration was calculable with the CaI_2 concentration determined by converting the corrected count-rate of the low energy X-ray range using Eq. 1. During the tracer experiment, at each selected x, measurements were repeated at a frequency of four to ten minutes to yield the profiles of the resident tracer concentrations.

The porosity and clay proportion scanned along the column C2 are given in Figure 2. The porosity appears to be relatively regular from the bottom up to 30 cm, with a value of 0.326 ± 0.015. It then increases to 0.38 for the last two centimetres. The clay fraction distribution followed the inverse trend of porosity distribution, the material being less dense in the upper part of the column. The average clay fraction was estimated at 0.208 ± 0.018. Despite a lower compaction state limited to the upper part of the column, the standard deviation of the clay fraction and porosity remained small. Consequently, the material filling this column can be considered as sufficiently well compacted to assume a homogeneous column for the modelling approach.

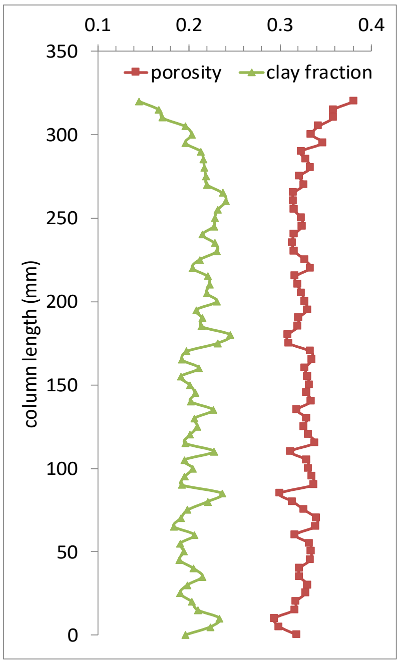

Figure 2: Porosity and clay content distribution in the column C2: the clay fraction is expressed as the ratio between the clay surface mass (g.cm^{-2}) and the sand surface mass (g.cm^{-2}), considering $\rho_{clay} = \rho_{sand} \sim 2.65$ g.cm^{-3}. Porosity is calculated as $\theta = 1 - \frac{\rho_i}{\rho_{CS}}$ with ρ_i the solid density measured at x_i and ρ_{CS} the grain density of CS (ca. ρ_{sand})

Because Ca is the major exchangeable cation in the natural material, and in order to study competition between Sr and Ca only, all columns were then saturated and Ca-conditioned by injection in the upward direction of around 800 v_p of de-aerated $CaCl_2$ 10^{-2} M solution (pH 6.5) at a constant flow rate (6-10 cm^3.h^{-1}). After saturation and conditioning, sorption sites of the clayey sandstone were mainly occupied by Ca^{2+} and H^+.

2.3.2 Operating and experimental conditions

After the conditioning step, a de-aerated 10^{-2} M $CaCl_2$ background solution was injected at a constant flow rate through the column in an upward direction. As steady flow was achieved, a tracer solution was also injected at the same steady flow rate through the column inlet; this was done by either using an injection loop filled with a tracer solution (columns C1 and C3) or by switching to a tracer bottle (column C2). A loop volume of 20.8 cm^3 containing tracer solutions was injected into column C1 and C3, whereas a volume of 2500 cm^3 was injected into column C2. The outflowing solution was collected as aliquots every 10 or 15 minutes depending on the flow rate to be analysed. The flow rate was controlled by weighing the collected aliquots. Moreover, the flow rate in column C2 was also controlled by weighing the inflow bottle during the experimental time. The non-reactive tracers chosen for these experiments were ^2H ($^2H/^1H = 2000$), Cl^- and I^- (10^{-1} M) in the centimetre-scale columns and I^- in the decimetre-scale column. In case of the inert CaI_2 tracer, the pH and electrical conductivity were monitored at the column inlet and outlet and the tracer concentration was recorded. The initial tracer solution contained a mixture of ca.10^{-4} M $SrCl_2$ and ca.10^{-2} M $CaCl_2$. The precise composition of the solutions used for each experiment was analytically controlled. No soluble natural Sr lixiviated from CS and Bt soil has been previously significantly measured by ICP/MS. Consequently, natural Sr was neglected in cation exchange process. The experimental parameters are summarised in Table 2.

Column	C1	C2	C3
Flow rate($cm^3.h^{-1}$) conservative tracer			
^2H	7.09 ± 0.68		7.21
	8.90 ± 0.36		8.43
	13.25 ± 0.29		
I^-	5.97 ± 0.20	51.93 ± 1.77	
		28.09 ± 1.79	
		27.28 ± 1.50	
		37.17 ± 1.60	
Cl^-	5.90 ± 0.34		
Flow rate($cm^3.h^{-1}$) Sr tracer	5.71 ± 0.18	19.86 ± 0.47	6.8 ± 0.22
	9.21 ± 0.28	27.21 ± 0.36	8.37 ± 0.49
	12.68 ± 0.21	38.24 ± 1.35	
	17.54 ± 0.31		
Dispersity[a] (cm)	0.24	0.28	0.33
Injection volume (cm^3)	20.8	2500	20.8
Material CEC (eq/kg)	0.064 ± 0.003	0.112 ± 0.006	0.13 ± 0.01[b]
% illite	5.84	10.14	4.73
%smectite	5.63	9.78	13.3

[a] Dispersivity determined from conservative tracer experiments

[b] Value provided by Lu *et al.* (2014)

Table 2: Operating conditions for conservative tracers and Sr transport experiments

3. Reactive transport modelling

As mentioned above, the objectives of this study are to evaluate the additive approach so as to simulate Sr transport in two-component materials. Thus, the experimental results were interpreted by coupling the multi-site ion exchanger model with a transport model.

3.1. Sr sorption model: a multi-site ion exchanger model

The multi-site ion exchanger model (MSIE) used in this study has already been described in detail by Motellier *et al.*, 2003; Jacquier *et al.*, 2004; Tertre *et al.*, 2009; Savoye *et al.*, 2012; Lu *et al.*, 2014, Reinoso-Maset and Ly, 2014, Siroux *et al.*, 2017, 2018 and Wissocq *et al.*, 2018. In this model, the ion-exchanger is composed of one or several negatively charged minerals. The latter typically have their own negative sorption sites (called X_i^-) able to sorb cations. The ion exchange models initially designed only allow the interpretation of ion exchange in terms of equilibrium and not reaction mechanisms. Thus, they consider that all sites behave indistinctly in the same way. For clay minerals, various adsorption sites result from isomorphic substitution of lattice cations and hydroxyl groups sensitive to pH. The sorption sites are distinguished by their exchange capacities CE_i without any structural assignment. Then, they are assumed as an intrinsic sorbent characteristic. Proton is the reference competing cation, due to its small size and its occurrence in solution. In this approach, the equilibrium expression below can be used to express the ion-exchange reaction related to the sorption site X_i with cations (M^{m+}), including H^+ selected as the reference (Eq. 2):

$$m\{(X_i^-) - H^+\} + M^{m+} = \{(X_i^-)_m - M^{m+}\} + mH^+ \qquad \text{(Eq. 2)}$$

with an associated apparent equilibrium constant (Eq. 3), the selectivity coefficient K^{i*} which includes the unknown activity coefficient of the adsorbed species (see Wissocq *et al.*, 2018), as defined as below:

$$K^{i*}_{mH^+/M^{m+}} = \frac{[(X_i^-)_m - M^{m+}]\,[H^+]^m (\gamma_{H^+})^m}{[(X_i^-) - H^+]^m\,[M^{m+}]\gamma_{M^{m+}}} \qquad \text{(Eq. 3)}$$

where *i* is the type of sorption site, [ ] is the concentration of species in solution (mol.L^{-1}) or sorbed species (mol.kg^{-1} of dry solid), and γ is the activity coefficient of the species in solution. In this study, the selectivity coefficient of Sr^{2+}/Ca^{2+} exchange is calculated for each site by combining $Ca^{2+}/2H^+$ and $Sr^{2+}/2H^+$ exchanges defined as follows:

$$K^{*i}_{Ca^{2+}/2H^+} = \frac{[X_i^- - H^+]^2[Ca^{2+}]\gamma_{Ca^{2+}}}{[(X_i^-)_2 - Ca^{2+}][H^+]^2\gamma^2_{H^+}} \qquad \text{(Eq. 4)}$$

$$K^{*i}_{Sr^{2+}/2H^+} = \frac{[X_i^- - H^+]^2[Sr^{2+}]\gamma_{Sr^{2+}}}{[(X_i^-)_2 - Sr^{2+}][H^+]^2\gamma^2_{H^+}} \qquad \text{(Eq. 5)}$$

The site capacity, CEi, is the sum of adsorbed species concentration per site (Eq. 6) and the sum of site capacities has to be equal to the CEC.

$$CE_i = 2[(X_i^-)_2 - Sr^{2+}] + 2[(X_i^-)_2 - Ca^{2+}] + [X_i^- - H^+] \qquad \text{(Eq. 6)}$$

Ca^{2+} selectivity coefficients are estimated for illite and smectite from Ca saturation curves as a function of pH. Saturation curves permit to quantify experimentally the exchange capacity of major sites, depending on their saturation evidenced by $Ca^{2+}/2H^+$ exchange. They express the adsorbed species concentration (mol/kg of solid) versus pH. Similarly, the minor site capacity is estimated on the Sr^{2+} adsorbed concentration versus Sr concentration curve. Reversible Sr adsorption reactions on Ca-illite and Ca-smectite have been verified experimentally by desorption experiments performed respecting the physico-chemical conditions of each adsorption experiments. This validates the adsorption/desorption reaction by cation exchange. Then, Sr^{2+} selectivity coefficients are estimated for illite and smectite from both pH and concentration sorption curves (Wissocq *et al.*, 2018). Equations 4, 5 and 6 are adjusted to the experimental adsorption isotherms by non-linear regression using Excel solver. Uncertainties on estimated selectivity coefficient were calculated by using the SolverAid macro De Levie (2004).

To apply this model on a natural soil or sediment by using a component additivity approach, it is assumed that the site capacities of the mineralogical assemblage are the sum of the site capacities of each reactive mineral component weighted by their relative abundance in the assemblage. In the two mineralogical systems selected for this study, illite and smectite mainly govern the sorption properties by ion-exchange processes. Consequently, the CEC of each material results on the contribution of illite and smectite and can be expressed by equation (7):

$$\mathrm{CEC}_{\mathrm{material}} = \sum_{\mathrm{i}}(\mathrm{x}_{\mathrm{illite}} * \mathrm{CEi}_{illite} + \mathrm{x}_{\mathrm{smectite}} * \mathrm{CEi}_{smectite}) \qquad \text{(Eq. 7)}$$

Where $\mathrm{x}_{\mathrm{illite}}$ and $\mathrm{x}_{\mathrm{smectite}}$ are the illite and smectite abundance in the material, and CEi_{illite} and $\mathrm{CEi}_{smectite}$ represent the illite and smectite $\mathrm{X}_{\mathrm{i}}^{-}$ site capacity respectively.

The selectivity coefficients of the mineralogical assemblage, restricted to a illite and smectite mixture, combine those which were determined on each site of pure illite and smectite in the batch experiments by Wissocq *et al.* (2018); they are summarised in Table 3. This multi-site ion exchanger model was implemented in the PHREEQC code using the EXCHANGE data block. Corrected selectivity coefficients obtained from the multi-site ion exchanger formalism were converted into the Gaines-Thomas formalism used by PHREEQC.

	Sites	CEi (eq/kg)	$LogK^{*i}_{2H^+/Ca^{2+}}$	$LogK^{*i}_{2H^+/Sr^{2+}}$	$LogK^{*i}_{Sr^{2+}/Ca^{2+}}$
Illite	Xh	0.001	-0.403 ± 1.977	1.700 ± 1.823	-2.103 ± 2.181
	Xa	0.131	-2.166 ± 0.073	-2.435 ± 0.64	0.269 ± 0.644
	Xb	0.043	-4.311 ± 0.216	-3.685 ± 0.367	-0.626 ± 0.626
	Xc	0.074	-11.745 ± 0.205	-11.25 ± 0.713	-0.495 ± 0.742
Smectite	Xe	0.387	-0.491 ± 0.486	-0.310 ± 0.028	-0.181 ± 0.485
	Xf	0.361	-4.352 ± 0.032	-4.475 ± 0.081	0.123 ± 0.087
	Xg	0.136	-14.837 ± 0.063	-14.778 ± 0.201	-0.059 ± 0.211

Table 3: Site names, capacities $\mathrm{CE_i}$ and selectivity coefficients $\mathrm{K}^{*\mathrm{i}}_{\mathrm{2H+/Ca2+}}$, $\mathrm{K}^{*\mathrm{i}}_{\mathrm{2H+/Sr2+}}$ and $\mathrm{K}^{*\mathrm{i}}_{\mathrm{Sr2+/Ca2+}}$ for Ca-illite and Ca-smectite (data acquired in batch experiments by Wissocq *et al.*, 2018).

The differences between $K^{*i}_{2H^+/Ca^{2+}}$ and $K^{*i}_{2H^+/Sr^{2+}}$ on the major illite sites are small given their uncertainties, only a significant difference is noticeable on the Xh site (Table 3). Consequently, the Sr selectivity compared to this of Ca is expressed by the negative value of $LogK^{*i}_{Sr^{2+}/Ca^{2+}}$. By neglecting this minor site X_h, the reactivity of Sr is comparable to that of Ca, as it is classically done by considering one site (Wahlberg *et al.* 1965). For smectite, the differences are not very significant according to the uncertainties of the selectivity coefficients. Therefore, the small difference in affinity between Sr and Ca is mainly due to the reactivity on X_h site of illite. This suggests that smectite plays a secondary role in the global reactivity of materials towards Sr.

3.2. Reactive transport model

Transport processes are computed via the advection-dispersion equation (ADE):

$$R_{(x)}\theta_{(x)}\partial_t C(x,t) = -\partial_x(q_{D(x)}C(x,t) - \theta_{(x)}D_{(x)}\partial_x C(x,t)) \qquad \text{(Eq. 8)}$$

With q_D representing the Darcy flow velocity (cm.h^{-1}), θ representing the porosity (-), C the solute concentration (mol.L^{-1}), R the retardation factor, and D the apparent dispersion coefficient (cm^2/h). The retardation factor can be calculated by the following equation:

$$R = 1 + \frac{\rho Kd}{\theta} \qquad \text{(Eq. 9)}$$

With ρ representing the mass density of solid and K_d the distribution coefficient.

R may depend on location *x* in the column when ρ and θ are spatially variable. However, in this study, we checked that the porous media were packed homogeneously and the transport parameters were considered uniform with *x*. Consequently, chemical retention can be expressed by Eq. 9 with a constant K_d. The retardation factor of a conservative tracer is equal to 1. The apparent dispersion coefficient is therefore calculated as follows:

$$D = \tau D_0 + \lambda v_{(x)} \qquad \text{(Eq. 10)}$$

With D_o being the molecular diffusion coefficient in free water (cm^2/h), τ the tortuosity (-), λ the dispersivity (cm), and *v* the pore velocity defined as $v(x) = \frac{q_D}{\theta(x)}$ (cm/h). The tortuosity was calculated following the Millington and Quirk (1961) equation.

The HYDRUS-1D code was used to simulate the conservative tracer experiments and the reactive transport experiment considering the constant K_d approach. Reactive tracer experiments were also simulated using the HP1 multicomponent transport module of HYDRUS-1D (Jacques and Simunek, 2010). This module couples HYDRUS-1D with the PHREEQC version 4 biogeochemical code (Parkhurst and Appelo, 1999).

The column geometry was modelled using a 1D Cartesian domain; columns C1 and C3 were discretized with 100 cells and column C2 with 350 cells. The columns were considered as physically and chemically uniform soil profiles. The water flux was used for the flow boundary condition. For conservative transport experiments and Sr transport in C1 and C3, the flow conditions imposed a dispersive hydrodynamic regime. For experiments in the C2 column, the slow flow velocities required taking into account a diffusion process. At the inlet, a constant tracer flux was imposed during the injection time and a zero-concentration gradient was selected as the outlet condition.

The input parameters measured experimentally were: dispersivity, porosity, flow velocity, solution compositions, and clay minerals characteristics relative to each material (site capacities, corrected selectivity coefficients). The molecular diffusion coefficients for Sr, Ca and Cl were $7.91\ 10^{-6}$, $7.92\ 10^{-6}$ and $2.03\ 10^{-5}$ $cm^2.s^{-1}$ respectively (Mills and Lobo, 1989).

Dispersivity was estimated by using: dedicated deuterated water (^2H), the $CaCl_2$ and CaI_2 transport experiment at centimetre scale (Table 2), and the CaI_2 transport experiment only at decimetre scale by using the Inverse module of HYDRUS-1D (Simunek *et al.*, 2008). The Levenburg–Marquardt algorithm was used to fit the nonlinear equations to experimental data.

The illite and montmorillonite characteristic inputs for simulations performed with HP1 take into account the respective site densities and selectivity coefficients weighted by the amount of every phase in each column. The solution compositions were: 10^{-2} M $CaCl_2$ as the background solution, and 10^{-4} M $SrCl_2$ and 10^{-2} M $CaCl_2$ for the tracer solution with a pH 7 (C3) or 6.5 (C1 and C2). The precise measured concentrations in each solution were implemented in the code for each experiment.

4 Results and discussion

4.1 Conservative transport

Non-reactive transport experiments were performed on the three columns before the Sr transport experiment to estimate the effective porosity available for transport and to determine the dispersivity independently from chemical retention.

4.1.1 Conservative transport at centimetre scale

The breakthrough curves (BTCs) of conservative, charged and neutral, tracers were acquired at varying flow rates in order to verify the flow independence towards preferential paths in the centimetre-scale columns C1 and C3. Figure 3 shows the BTCs as concentrations normalised to the injected concentration (C_0) versus volume of solution flowing through the column normalised to the column pore volume (v_p). In this way, it is possible to compare the results on a single plot. In the case of column C1, the BTCs resulting from the three conservative tracers overlap with one another (Figure 3a). Anion exclusion process and dual porosity can therefore be excluded, and the accessible porosity can be assimilated to the total porosity. Similarly for column C3 (Figure 3b), the ^{2}H BTCs are superimposed for both flow velocity. This justifies considering the total porosity to describe transport in the centimetre-scale Bt soil column (C3) and the CS column (C1).

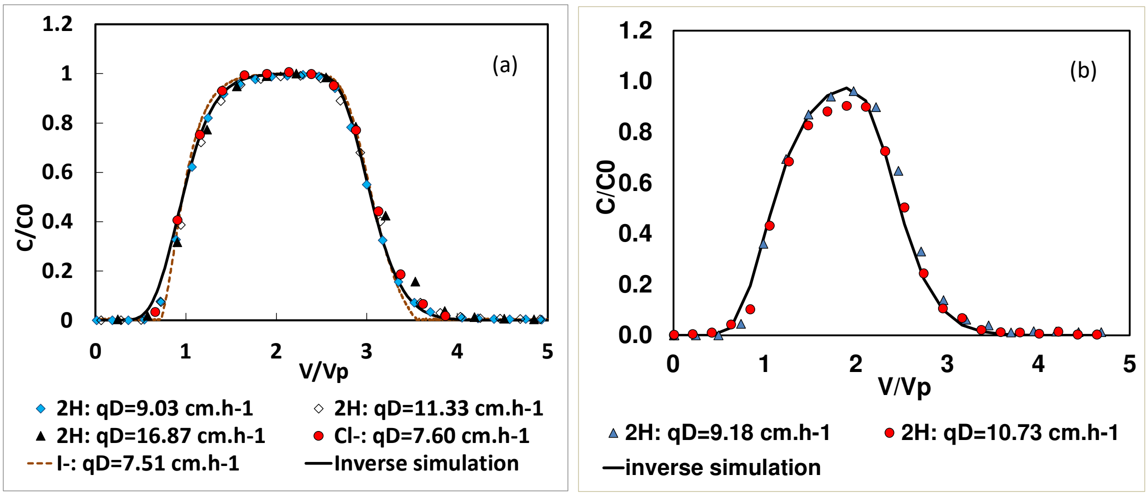

Figure 3: Conservative transport in (a) column C1 and (b) column C3. The inverse simulation results are displayed with a black line.

The total porosity and experimental flow velocity were used in the inverse module of Hydrus-1D to calculate the longitudinal dispersivity by way of adjustment with the experimental BTCs. The dispersivity values obtained were 0.24 ± 0.01 and 0.33 ± 0.02 cm for column C1 and C3 respectively ($R^2 = 0.998$).

4.1.2 Conservative transport at decimetre scale

Conservative transport experiments were performed with a CaI_2 tracer in column C2. Four tracer injections were conducted at various flow velocities to acquire the CaI_2 concentration curves at eight locations along the column and the BTCs at the column inlet and outlet (Figure 4). As in the centimetre-scale columns, the total porosity and measured flow velocities were chosen as input parameters for the inverse modelling on the complete set of resident concentration curves, simultaneously. The dispersivity was then estimated by inverse modelling. Finally, the resulting simulations show good agreement with the resident concentration curves. A slightly larger dispersion can be observed in the curve at the outlet, which is attributable to extra-column artefacts due to the presence of the filter with different transport properties. The average dispersivity was estimated at 0.323 ± 0.014 cm ($R^2 = 0.975$) in the decimetre-scale column considering the four experiments. By overlapping the simulations with data, it becomes evident that a unique set of total porosity, flow rate and dispersivity values are necessary to successfully simulate the resident concentration curves simultaneously at the eight locations along column C2. These results support the assumption of a continuous and homogeneously packed medium.

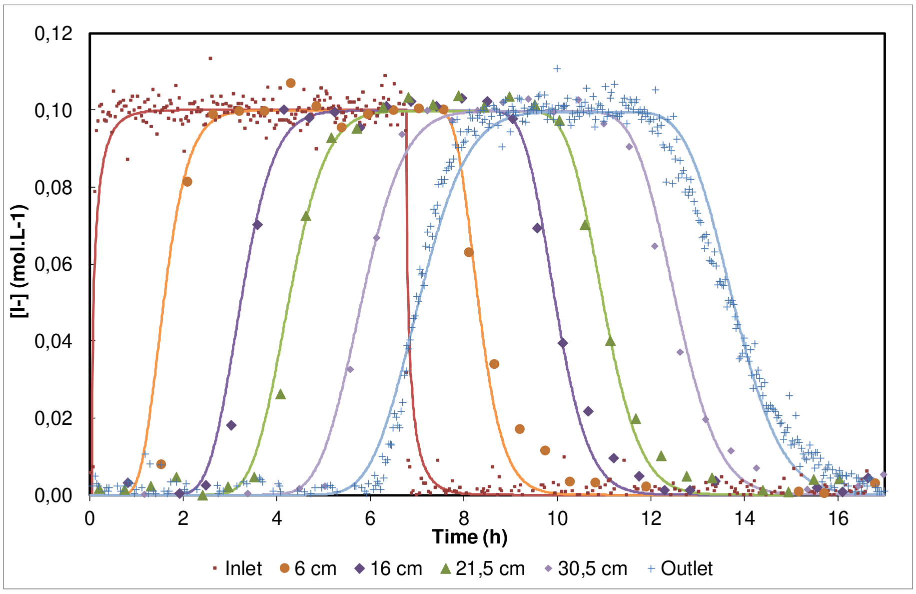

Figure 4: Experimental iodide concentration versus time recorded at 4 of the 8 locations (x = 6 cm, 16 cm, 21.5 cm and 30.5 cm from the column bottom) along column C2; inlet (red) and outlet (blue) BTCs of the CaI_2 tracer. The solid lines indicate the simulation curves

4.2 Sr reactive transport in a clayey sand

In order to compare the additivity approach with the commonly used K_d approach, simulations were carried out to interpret the experimental BTCs acquired on the CS material in the centimetre-scale column.

4.2.1 Tentative interpretation using a constant K_d

A retardation factor based on a constant K_d was tested to interpret Sr reactivity, specifically on the CS material. It is generally admitted that Sr is characterized by a linear isotherm (Wissocq et al., 2018, Rafferty et al., 1981). Wissocq *et al.* (2018) evidenced constant K_d values for Sr concentrations in solution up to 10^{-3} M in the case of Sr sorption on the CS material. Moreover, Szenknect *et al.* (2005) pointed out that, based on the flow-through reactor study, the K_d value was constant for Sr concentrations below 10^{-6} mol.L^{-1}. The isotherm described by the Langmuir model shows that a nonlinear, instantaneous and reversible sorption process controls Sr chemical reactivity. The Sr adsorption kinetics studied by Galambos *et al.* (2013) on clay mixtures evidenced an adsorption equilibrium achieved in one minute. The Sr adsorption reaction can be considered faster than the contact time in our transport experiments.

Four Sr BTCs were acquired on column C1 at varying flow velocities (Table 3). In Figure 5, the four normalised BTCs overlap with each other, indicating that Sr transport is independent from the flow rate in this context. The symmetric BTCs confirm the absence of a sorption kinetic effect on Sr transport in these experimental conditions. Direct simulations were conducted using the K_d based on batch sorption experiments (Wissocq *et al.*, 2018) and the K_d estimated from inverse modelling. Both simulation curves reproduced the BTCs experimental shapes well. This indicates that Sr and conservative tracers migrate through the material using the total porosity and the same transport pathways (i.e. same dispersivity as for the tracers). The K_d fitted on the experimental data was 3.64 $L.Kg^{-1}$, similar to the mean K_d estimated by batch experiments (3.68 ± 0.4 $L.Kg^{-1}$). Hence, site availability in compacted media remains the same as in dispersed material. The simulated curves overlap the data although the maximum intensity of the peak was not reached. Maximum and minimum batch K_d values (3.28 and 4.09 $L.Kg^{-1}$ respectively) were also tested to estimate the K_d variability on the simulation results. The experimental data lie well between the two curves, except for a few points at the maximum concentration. When considering the minimum batch K_d, the simulated curve recorded an earlier arrival and higher intensity than the curve obtained by inverse modelling. Accordingly, the simulated curve with the maximum batch K_d revealed a lower intensity and a longer residence time in the column. This confirms that K_d is a highly sensitive parameter when it comes to simulating reactive transport in columns. Consequently, K_d determined in static conditions may be used to describe Sr transport in the CS material if uncertainties can be tolerated (safety criteria for instance).

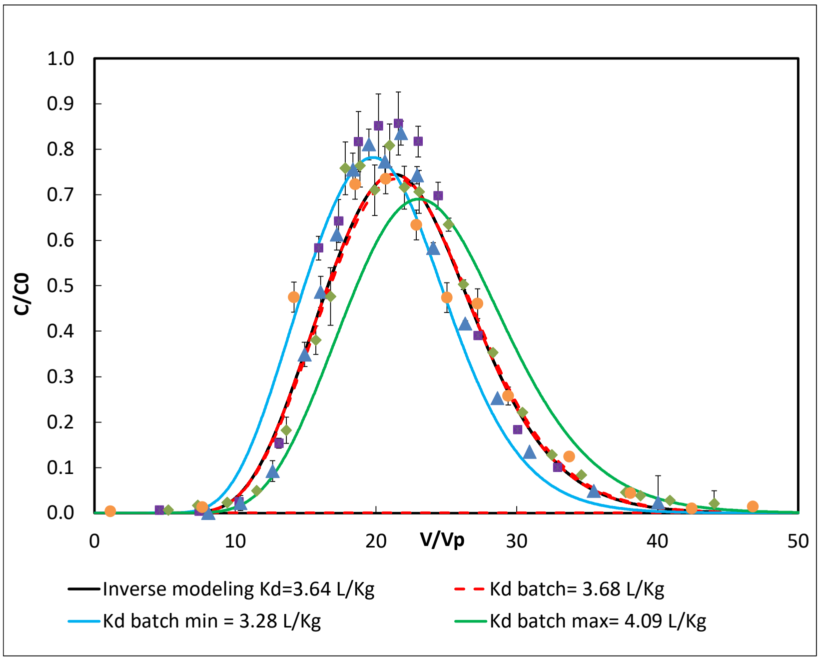

Figure 5: Sr breakthrough curves acquired at different flow velocities in column C1 (data points: purple squares at 7.27 cm.h^{-1}, blue triangle at 11.73 cm.h^{-1}, green diamonds at 16.14 cm.h^{-1} and orange circles at 22.33 cm.h^{-1}) and compared with direct modelling results obtained with the batch K_d (solid and dashed lines).

4.2.2 Additivity approach using a multi-site cation exchanger model

In order to explain the role of the different clay minerals in Sr transport, simulations were conducted using the additivity of the illite and smectite sorption properties and considering their relative abundances in porous media. Wissocq *et al.* (2018) successfully applied an additivity approach with a multi-site ion exchanger model (MSIE) based on a mixture of pure mineral phases (illite and smectite) to simulate Sr sorption on the CS material in batch experiments. This approach was therefore adopted in our work to simulate Sr transport through CS columns by coupling the MSIE model with the transport model (ADE). Transport parameters such as total porosity and dispersivity deduced from transport experiments using conservative tracers, were once again used for the simulations. The sorption properties of reactive phase-type (illite or smectite) and their abundance in the material are hence two determining parameters. In the centimetre scale column, the clayey sandstone was assumed to behave like a homogeneous media. Therefore, our approach first focuses on the mineral specificity.

For this purpose, it is generally admitted that three major sorption sites are necessary to describe the illite and smectite exchange capacity (Nolin, 1997, Tertre *et al.*, 2009, Wissocq *et al.*, 2017). The sorption properties of CS are assumed analogue to those of an illite and a smectite phases mixture. However, Wissocq *et al.* (2018) obtained a better interpretation of the Sr sorption curves on pure illite in batch experiments by considering a fourth site: a low-capacity and high-affinity site. Such low-capacity sites are recognised to act principally at low concentration and represent less than 0.5 % of the total exchange capacity of the clay mineral (Brouwer *et al.*, 1983; Baeyens and Bradbury, 1997; Poinssot *et al.*, 1999; Missana *et al.*, 2004, 2008; Tertre *et al.*, 2009, Martin *et al.*, 2018, Latrille *et al.*, 2019). On another hand, Sr sorption isotherms on smectite did not reveal the contribution of this kind of site. The significance of X_h site on Sr transport is therefore investigated by comparing simulation including or not the X_h site.

Following the literature, the simulations were firstly carried out with the three major sites for illite (X_a, X_b, X_c) and smectite (X_e, X_f, X_g). Their specific features are given in Table 3. Simulations results obtained on column C1 are shown in Figure 6. Compared with experimental BTCs, the simulated curve indicates a slightly earlier arrival time in column C1 conserving the BTCs' rather symmetrical shape and fit in the experimental data range.

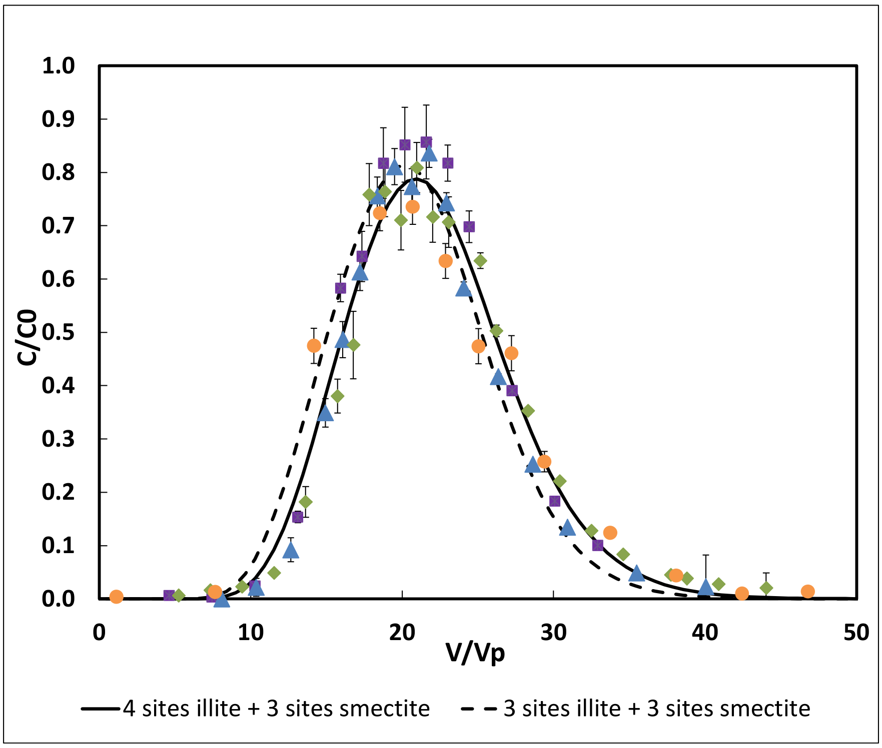

Figure 6: Sr breakthrough curves acquired at different flow velocities (points) in column C1 compared with direct modelling results. Simulation considers three sites for smectite and three (dashed curve) or four sites for illite (solid black line).

To assess the influence of the minor site in Sr transport, sensitivity calculations were performed including the fourth site (X_h) on illite (Figure 6). Again, the simulated curve was correctly superimposed on the Sr breakthrough curve in the CS column and reproduced the BTCs' shape, leading to a slightly better fit with respect to the maximal intensity and the short tail.

4.2.3 Sr reactive transport on a decimetre scale

The effect of the mineral abundance on the Sr transport results was tested on a larger column scale. Local stacking heterogeneities of small extent (± 2% of clay content) were recorded during the decimetre-column filling process (Figure 2). They express the clay fraction variability along the column. The grain-size fractionation uncertainty was around 2%. This implies a CEC variation in the filling material of ± 0.012 eq.kq^{-1}, which equates to a variability in sorption capacity (i.e. in number of site). Only the cumulative effect of variations in the clay fraction could be tested, given that Sr BTCs were only available at the column outlet. Simulations were therefore carried out at various averaged clay fraction contents and then compared with the experimental data in order to test the sensitivity of simulation outcomes to CEC variability.

Sr transport experiments were also performed on decimetre-scale columns (C2) filled with same material and applying three different flow rates (Figure 7). The resulting BTCs are well superimposed, as in the case of the centimetre-scale column. In the modelling, we considered that the porous medium was homogeneous, even though small-scale heterogeneities were detected on the porosity and clay proportion distribution (Figure 2). The measured flow rate, an averaged total porosity and dispersivity were used as input parameters for simulations with the HP1 and HYDRUS 1D codes. As for column C1, direct simulations with HYDRUS 1D were conducted using the Kd value based on batch sorption experiments (Kd = 6.44 L/kg), in Fig. 7. The simulated curve with Kd overlaps well with the data in terms of arrival time and tail, but not so well with the maximal intensity of the peak. Then, MSIE model was tested to improve the simulation outcomes. The C2 column reactivity was simulated using the sorption parameters relative to illite and smectite, weighted by their relative abundance in the material. The average clay proportion, estimated at ca. 20% by dichromatic X-ray spectrometry (Figure 2), was taken into account to calculate the sorption parameters of the CS material by considering three sites for smectite and four sites for illite with HP1. The simulation results in Figure 7 are in good agreement with the experimental Sr BTCs. As observed in the C1 column, there was no visible broadening of the Sr tracer curve. Theoretically, upscaling the column size has no impact on the Sr transport in the case of a homogeneous porous medium containing easily accessible sorption sites.

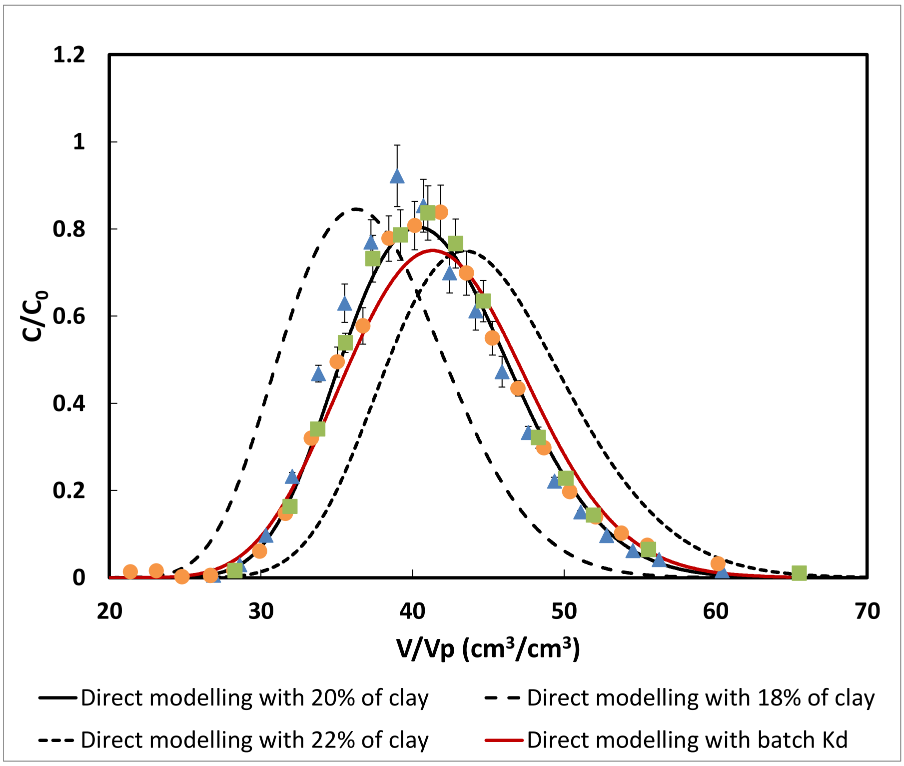

Figure 7: Sr breakthrough curves acquired in the decimetre column (C2) at flow rates of 1.95 cm.h^{-1} (orange circles), 1.39 cm.h^{-1} (green squares) and 1.01 cm.h^{-1} (blue triangles). The simulation results obtained with 22 % of clay (dotted line), 20 % of clay (solid line) and 18 % of clay (dashed line) by considering three sites for smectite and four sites for illite. Direct modelling results with the batch K_d value at 6.44 L.Kg^{-1} (red line).

To assess the sensitivity of clay content variability, two additional simulations were performed considering 18% and 22% clay fractions (Figure 7) with HP1. The results indicate an earlier arrival and retardation of the front respectively, the whole curves being shifted in time. This small uncertainty was also sensitive for the arrival time of the front. Overall, the reactive transport model successfully predicts the Sr reactive transport through the clayey sandstone on a decimetre scale with transport parameters and chemical retention based on clay mineral contributions that have been determined experimentally. Independently from the relative abundance of the clay minerals, the clay fraction in each column appears to have a strong impact on the modelling outcome. This may explain the difficulty of simulating transport on a field scale where the heterogeneity of porous media can be more marked.

4.3 Sr reactive transport in a Bt soil horizon

In order to explore the scope of this approach, a similar study was replicated in another column filled with a different material. Two Sr BTCs were acquired on the Bt soil horizon (column C3, Latrille *et al.*, 2017) under operating conditions comparable to those of column C1. Expressed in normalised concentration vs. normalised flowing volume over pore volume, the data obtained with two different flow velocities once again overlapped each other (Figure 8) and show spreading curves with a larger tail than the Sr BTCs for CS material (Figure 6). The BTCs indicate the same relative arrival time as that of column C1, corresponding to the injection of ten pore volumes (v_p), but they differ in intensity and tail length. The geometrical features of both columns are comparable and cannot be invoked to explain the difference in the intensity of the BTCs. Nonetheless, both materials have a distinct CEC: 0.064 eq/kg in column C1 compared with 0.13 eq/kg in column C3. These CEC values represent the respective illite and smectite contributions in each porous medium. As detailed in Table 2, the illite and smectite contents are similar in the CS material, whereas the illite-to-smectite ratio is 0.35 in the Bt soil.

4.3.1 Kd and MSIE modelling results

In Figure 8, the simulated curve (black solid line) was obtained by inverse modelling using the experimental flow velocities, total porosity and dispersivity. The optimized K_d was found to be 7.5 L.Kg^{-1} ($R^2 = 0.949$). This curve does not fit the experimental data satisfactorily, showing a delayed maximum value and a shorter tail.

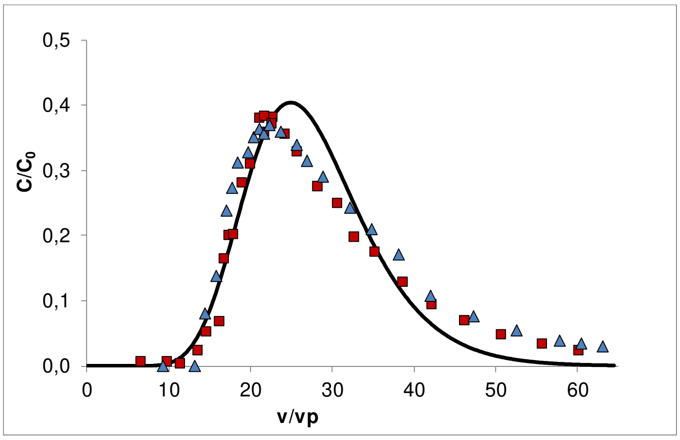

Figure 8: Sr breakthrough curves in Bt soil in column C3 obtained with flow velocities of 8.66 cm.h^{-1} (red squares) and 10.66 cm.h^{-1} (blue triangles) and the dispersivity determined with a conservative tracer at 0.33 cm. Inverse modelling simulation given a K_d optimised at 7.50 L.Kg^{-1} (black line)

The presence of a tail in the BTC could be attributable to transport mechanisms (double porosity or intra-particle diffusion) or chemical mechanisms (kinetic control of sorption/desorption, sorption site parameters). We discarded transport based on the results obtained with conservative tracers (single porosity), which show no such tail in the BTCs. Based on Galambos *et al.* (2013) and Siroux *et al.* (2017), kinetic effects may also be excluded. Indeed, the results of these studies evidenced Sr sorption achieved at shorter time (about seconds to hours, respectively) than the experimental time scale of our study. In order to reduce the mismatch between simulation and experimental data and to explain the dissymmetry of the BTC, additional simulations were therefore conducted to test the additivity approach with the MSIE model. The simulation results (Figure 9) obtained with the parameters described above (three or four sorption sites on Ca-illite) do not improve the mismatch. They show an early arrival time, a larger intensity and a depleted tail (small squares and crosses in Figure 9). Further sensitivity calculations on the variability of the clay fraction (in the uncertainty range, i.e. 17 % to 19.4 % of < 2 µm) indicate a significant shift in time towards an earlier breakthrough, a higher maximal value, and symmetrical curves without any tail (SI2). As a result, the clay mineral amount does not explain the late arrival and length of the tail. The relative abundance of illite and smectite was also tested in the range of uncertainties observed by the CEC and XRD quantifications. Obviously, the relative proportions of illite and smectite are so strongly constrained that the simulation results reveal no significant enhancement (SI3).

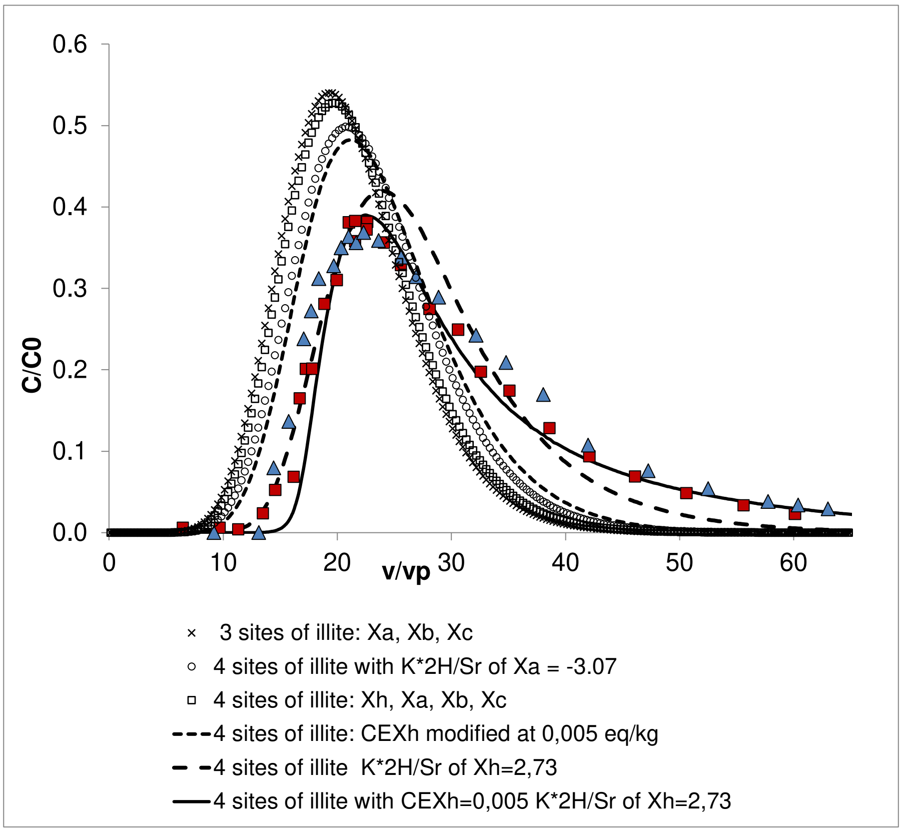

Figure 9: Sr breakthrough curves acquired on the Bt soil (column C3) at two different flow velocities (blue and red points). The simulation considers the dispersivity determined with a conservative tracer at 0.33 cm and 18 % of clay content.

The sensitivity calculations were therefore extended to the parameters of sorption sites, focusing on the illite, to investigate their influence on Sr transport (considering the lower uncertainty on site selectivity coefficients of montmorillonite) (Table 3). The additional simulations involved the selectivity coefficient of the major site X_a for Ca-illite, which shows the largest uncertainty, as well as both the selectivity coefficient and exchange capacity, which are characteristics of the highest selective site X_h (Figure 9). When the selectivity coefficient of X_a is increased to the highest eligible value in the uncertainty range, $K^{*Xa}_{2H+/Sr2+}$ = -3.075, the curve shows a slight shift in time and the intensity decreases, but not enough to match the experimental data (circles in Figure 9). A similar result was obtained when the CE_{Xh} value was increased to 0.005 eq/kg (dotted line in Figure 9). This shows that the major site selectivity coefficient and the CE_{Xh} values are not solely responsible for the large tail. When the simulation was conducted with an increased selectivity coefficient (representing

0.5 σ), $K^{*Xh}_{2H+/Sr2+}$ = 2.73 (Table 3), a slight improvement could be observed with a breakthrough time closer to the observations, but still not matching the tail (dashed line in Figure 9). It is only by increasing both the site capacity CE_{Xh} to 0.005 eq/kg and the selectivity coefficient from 0.5 σ that the simulated curve adequately superimposes with the experimental data (solid line in Figure 9). It appears that the low-capacity and high-affinity sites of illite are key to widespread dispersion and tailing during Sr transport in this soil column.

4.3.2 Discussion on the Bt soil results

The overall results suggest that Sr transport in these experiments occurs without limitation imposed by site accessibility as suggested by the superimposed BTCs for the two flow velocities and the matching arrival time of the simulated curve with the K_d approach. In the case of the Bt soil, the BTC curves show a marked tail that is more difficult to capture with the models. As suggested by Bugai *et al.*, (2012, 2020), a Kd approach is unable to predict the impact of chemical disturbances in case of mixed cation competition. In the same way, Vulava *et al.* (2000) have already studied cation exchange equilibria between the two major cations in a natural soil material by assimilating its retention properties to one-site. They evidenced that classical one-site cation exchange equations do not accurately describe cation exchange isotherms over a wide range of concentrations. In the same line, Missana *et al.* (2008) recommended the description of radionuclide retention by a mechanistic approach rather than distribution coefficient. Another hypothesis is that other minor reactive components in the soil may influence the sorption of Sr.

The low soil organic matter content in this soil sample (0.34 %) and its small influence on Sr adsorption (Samadfam *et al.*, 2000) lead us to disregard its contribution to Sr transport in the Bt soil column.

Ferrihydrite is also frequently encountered in this type of soil. Hofmann *et al.* (2005) noticed significant Sr adsorption on ferrihydrite at pH 7 (conditions close to our experiment pH~7), i.e. 4.5 10^{-6} mol of Sr per gram of ferrihydrite. Considering the 2.27% of iron of the Bt soil horizon (Lamy *et al.*, 2006) attributed to iron oxide, it can be converted into 3.6 wt% of ferrihydrite (Lu, 2015). The ability of this oxide to capture Sr in the column C3 (i.e.; 0.32 g of ferrihydrite) yields 1.46 10^{-6} mol of Sr compared with 5.2 10^{-2} mol of Sr introduced, which is equivalent to a capture rate of 0.03 for one thousand. Despite the negligible contribution of this minor mineral on Sr sorption, our modelling approach will gain from being refined with available data that can be interpreted using our formalism.

The simulation results obtained by coupling the MSIE model with ADE therefore focused on the sorption on clay minerals. These results reinforce the robustness of the additivity approach and the parameters for the sedimentary rock (CS material), but are limited in the predictive capacity of the modelling for the Bt soil. One of the sorption properties of the illite site needed to be adjusted in order to simulate Sr transport behaviour in the soil. This highlights the difficulty of assimilating the sorption properties of soil clay minerals (illite from the Bt soil) with respect to those of sedimentary clay minerals (illite from the Puy region). Several explanations can be proposed for this behaviour. Firstly, the exchange capacity of the low-capacity and high-affinity sites of illite (denoted here CE_{Xh}) was previously estimated by other authors with various trace elements (Poinssot *et al.*, 1999, Missana *et al.* 2008, 2014, Altmann *et al.*, 2015, Martin *et al.*, 2018, Latrille *et al.*, 2019). This value was found only by adjusting the Sr sorption curves to 0.005 eq/kg in Wissocq *et al.*, (2017) and 0.002 eq/kg in Altmann *et al.* (2014) and 0.0027 eq/kg in Latrille *et al.*, 2019 to model Zn sorption on Na-illite and Ca-illite respectively. Lower values were also found by Poinssot *et al.* (1999), i.e., 0.0005 eq/kg for Cs sorption on Na-illite, which is close to that determined by Missana *et al.* (2014) for Cs sorption on Ca-illite (i.e. 0.0003 eq/kg) and Martin *et al.* (2018) for Tl sorption on Ca-illite (i.e. 0.00025 eq/kg). Such differences evidence the difficulty of constraining this low-capacity site with good accuracy. Secondly, clay minerals in soil are commonly encountered in a wide range of particle sizes from 50 nm to 5 µm (Hubert et al, 2012), i.e. a finer size than in sedimentary clay. Inherent to their high specific surface and CEC (Reinholdt *et al.,* 2013), the finest particles have a larger ability to adsorb. In this respect, we know that illite can be weathered or micro-divided due to pedogenic processes. In soil environments, illite may contain a larger amount of low-capacity and high-selectivity sites (commonly referred to as frayed edge sites) attributed to particle edges (Sawhney, 1972), and fewer sites located on the basal surface and in the interlayer space. As a result, the reactivity of soil illites is enhanced compared with sedimentary clay mineral like illite du Puy and illite contained in the CS material. This assumption is consistent with the simulation results obtained by adjusting the capacity and affinity of the fourth site on illite in the Bt soil.

4. Conclusion

In this study, we coupled the multi-site ion exchanger model (MSIE) based on a component additive approach, with the advection-dispersion equation (ADE). We did this to assess how well it would be able to simulate Sr reactive transport in two materials, a clayey sandstone and a Bt soil. Non-reactive transport experiments performed with conservative tracers were first used to determine the transport parameters, such as porosity and dispersivity. This reactive transport model was tested to simulate Sr transport data acquired in a centimetre- and a decimetre-scale column. Although the K_d approach is able to describe Sr sorption in static conditions (batch) and remains applicable in dynamic conditions for the CS material (given the K_d value uncertainty), it is less efficient at reproducing experimental data in the column for the Bt soil. Using the additivity approach and considering components described by multi-sorption sites, the reactive transport of Sr in the clayey material CS can be successfully predicted on a centimetre- and decimetre-scale without adjusting any of the parameters (those measured in batch experiments). Sensitivity parameter tests revealed the noticeable impact of the clay content and mineralogical characteristics on Sr transport simulations. These results highlight the influence of illite on Sr BTC spreading, especially through its low-capacity and high-selectivity site. This implies having access to a robust and extensive database established with reference minerals. The results of this study confirm the robustness of our database when clay minerals have reactivity properties similar to those of the reference minerals employed to build the database. In the case of the Bt soil containing weathered mineral or evolved minerals, this database appears more limited and needs to be perfected. The choice of modelling approach is therefore crucial when modelling and predicting the behaviour of Sr transport in porous media. To consolidate the robustness of this approach, it would be relevant to test it on heterogeneous media and to acquire retention properties of weathered illite. Moreover, a systematic sensitivity analysis would also be interesting, potentially unraveling a combined effect of different parameters.

Acknowledgment

We would like to thank P. Fichet for the ICP-MS analysis and Etudes Recherches Matériaux (Poitiers, France) for the XRD quantification of the mineral phases in the CS material.

Funding: This work was 100% financed by the MRISQ project at the CEA.

References

Altmann, S., Aertsens, M., Appelo, T., Bruggeman, C., Gaboreau, S., Glaus, M., Jacquier, P., Kupcik, T., Maes, N., Montoya, V., Rabung, T., Robinet, J-C., Savoye, S., Schaefer, T., Tournassat, C., Van Laer, L., Van Loon, L., 2014. Processes of cation migration in clayrocks, CatClay Final Scientific Report D1.6.

Aplin, A.C., Matenaar, I.F., McCarty, D.K. & Van Der Pluijm, B.A., 2006. Influence of mechanical compaction and clay mineral diagenesis on the microfabric and pore-scale properties of deep-water Gulf of Mexico mudstones. Clays & Clay Minerals, 54, 500–514. https://doi.org/10.1346/CCMN.2006.0540411

Appelo, C.A.J., 1994. Some calculations on multicomponent transport with cation-exchange in aquifers. Ground Water 32, 968-975.

Bachhuber, H., Bunzl, K., Schimmack, W., Gans, I., 1982. The migration of ^{137}Cs and ^{90}Sr in multilayered soils: results from batch, column, and fallout investigations. Nuclear Technology 59, 291-301.

Baeyens, B., Bradbury, M.H., 1997. A mechanistic description of Ni and Zn sorption on Na-montmorillonite. Part I: Titration and sorption measurements. J. Cont. Hydrol., 27, p. 199-222.

Berns, A., E., Flath, A., Mehmood, K., Hofmann, D., Jacques, D., Sauter, M., Vereecken, H., Engelhardt, I., 2018. Numerical and experimental investigations of caesium and strontium and transport in agricultural soils. Vadose zone J. 17:170126. https://doi.org/10.2136/vzj2017.06.0126.

Bradbury, M. H., Baeyens B., 2000. A generalized sorption model for the concentration dependent uptake of caesium by argillaceous rocks. Journal of Contaminant Hydrology 42, 141-163.

Bouchet, A., 1992. Mise au point d'un programme de détermination automatique des minéraux argileux. Comptes Rendus du Colloque de Rayons X-Siemens 2, 52-61.

Bugai, D., Skalskyy, A., Dzhepo, S., Kubko, Y., Kashparov, V., Van Meir, N., Stammose, D., Simonucci, C., Martin-Garin, A., 2012. Radionuclide migration at experimental polygon at Red Forest waste site in Chernobyl zone. Part 2: Hydrogeological characterization and groundwater transport modelling. Appl. Geochem. 27, 1359–1374, https://doi.org/10.1016/j.apgeochem.2011.09.028.

Bugai. D., Smith, J., Hoque, M.A., 2020. Solid-liquid distribution coefficients (Kd-s) of geological deposits at the Chernobyl Nuclear Power Plant site with respect to Sr, Cs and Pu radionuclides: A short review. Chemosphere 242, 125175. https://doi.org/10.1016/j.chemosphere.2019.125175

Brouwer, E., Baeyens, B., Maes, A., Cremers, A., 1983. Cesium and rubidium ion equilibriums in illite clay. The J. Phys. Chem. 87, p. 1213-1219.

Cui, D., Eriksen, T.E., 1998. Reactive transport of Sr, Cs and Tc through a column packed with fracture-filling material. Radiochim. Acta 82, 287–292.

De Levie, R., 2004. Advanced Excel for Scientific Data Analysis. Oxford, UK: Oxford University Press. 625 p.

Fesch, C., Simon, W., Haderlein, S.B., Reichert, P., Schwarzenbach, R.P., 1998. Nonlinear sorption and nonequilibrium solute transport in aggregated porous media: Experiments, process identification and modelling. J. Contam. Hydrol. 31, 373-407.

Galambos, M., Krajnak, A., Rosskopfova, O., Viglasova, E., Adamcova, R., Rajec, P., 2013. Adsorption equilibrium and kinetic studies of strontium on Mg-bentonite, Fe-bentonite and illite/smectite. J. Radioanal. Nucl. Chem., 298, 1031-1040. https://doi.org/10.1007/s10967-013-2511-1.

Hayes, K.F., Leckie, J.O., 1987. Modeling ionic strength effects on cation adsorption at hydrous oxide/solution interfaces. J. Colloids Interface Sci., 115(2), 564-572.

Hofmann A., van Beinum W., Meeussen J.C.L., 2005. Sorption kinetics of strontium in porous hydrous ferric oxide aggregates II. Comparison of experimental results and model predictions. J. Colloid Interface Sci. 283, 29-40. http://doi.org/10.1016/j.jcis.2004.08.105.

Hölttä, P., Siitari-Kauppi, M., Hamanen, M., Huitti, T., Hautojärvi, A., Lindberg, A., 1997. Radionuclide transport and retardation in rock fracture and crushed rock column experiments. J Contam Hydrol. 26, 135–145.

Hubert, F., Caner, L., Meunier, A., Ferrage, E., 2012. Unraveling complex <2µm clay mineralogy from soil using X-ray diffraction profile modeling on particle-size subfractions: Implications for soil pedogenesis and reactivity. Am. Mineral. 97, 384-398. http://dx.doi.org/10.2138/am.2012.3900

Jacques, D., Šimůnek, J., 2010. Notes on HP1, a software package for simulating variably-saturated water flow, heat transport, solute transport, and biogeochemistry in porous media, HP1 Version 2.2., Open Report, SCK•CEN-BLG-1068, Mol, Belgium.

Jacquier, P., Ly, J., Beaucaire, C., 2004. The ion-exchange properties of the Tournemire argilite I. Study of the H, Na, K, Cs, Ca and Mg behaviour. Appl. Clay Sci. 26, 163–170. https://doi.org/10.1016/j.clay.2003.09.009

Kashparov, V.A., Lundin, S.M., Zvarych, S.I., Yoshchenko, V.I., Levchuk, S.E., Khomutinin, Y.V., Maloshtan, I.M., Protsak V.P., 2003. Territory contamination with the radionuclides representing the fuel component of Chernobyl fallout. Sci. Total Env. 317, 105–119. https://doi.org/10.1016/S0048-9697(03)00336-X

Lamy, I., van Oort, F., Dère, C., Baize, D., 2006. Use of major- and trace-element correlations to assess metal migration in sandy Luvisols irrigated with wastewater. Eur. J. Soil Sci. 57, 731-740. https://doi.org/10.1111/j.1365-2389.2005.00765.x

Latrille, C., Cartalade, A., 2010. New experimental device to study transport in unsaturated porous media. Water Rock Interaction 13- Birkle & Torres-Alvarado (eds) Taylor & Francis Group, Balkema Proceeding and Monographs in Engineering, Water and Earth Sciences, 299-302.

Latrille, C., Néel, M.C., 2013. Transport study in unsaturated porous media by tracer experiment in a dichromatic X-ray experimental device. EPJ Web of Conferences 50, 04002, https://doi.org/10.1051/epjconf/20135004002

Latrille, C., Wissocq, A., Beaucaire, C., Siroux, B., 2017. Simulation of Sr transport in soil column. Procedia Earth and Planetary Science 17, 476-479. https://doi.org/10.1016/j.proeps.2016.12.120

Latrille, C., Wissocq, A., Beaucaire, C., 2019. Zn sorption on Ca-illite and Ca-smectite: experiment and modelling. E3S Web of Conferences 98, 04008 . https://doi.org/10.1051/e3sconf/20199804008

Lichtner, P.C., Yabusaki, S., Pruess, K., Steefel, C.I., 2004. Role of competitive cation exchange on chromatographic displacement of cesium in the vadose zone beneath the Hanford S/SX tank farm. Vadose Zone J. 3, 203-219. https://doi.org/10.2136/vzj2004.2030

Liu, D., Jivkov, A. P., Wang, L., Si, G., Yu, J., 2017. Non-Fickian dispersive transport of strontium in laboratory-scale columns: Modelling and evaluation. J. Hydrol. 549, 1-11. https://doi.org/10.1016/j.jhydrol.2017.03.053

Lu, J., Tertre, E., Beaucaire, C., 2014. Assessment of a predictive model to describe the migration of major inorganic cations in a Bt soil horizon. Appl. Geochem. 41, 151-162. http://dx.doi.org/10.1016/j.apgeochem.2013.12.009

Martin, L.A., Wissocq, A., Benedetti, M.F., Latrille, C., 2018. Thallium (Tl) sorption onto illite and smectite: implications for Tl mobility in the environment, Geochim. Cosmochim. Acta 230, 1-16. https://doi.org/10.1016/j.gca.2018.03.016

Millington, R.J. and Quirk J.M., 1961. Permeability of porous solids. Trans. Faraday Soc., 57:1200-1207.

Mills, R., Lobo, V.M.M., 1989. Self-diffusion in electrolyte solutions: a critical examination of data compiled from the literature, Elsevier, Amsterdam. 346p.

Missana, T., Garcia-Gutierrez, M. Alonso, U., 2004. Kinetics and irreversibility of cesium and uranium sorption onto bentonite colloids in a deep granitic environment. Appl. Clay Sci. 26, 137–150. https://doi.org/10.1016/j.clay.2003.09.008

Missana, T., Garcia-Gutiérrez, M., Alonso, U., 2008. Sorption of Sr onto illite/smectite mixed clays. Phys. Chem. Earth 33, S156-S162. https://doi.org/10.1016/j.pce.2008.10.020

Missana, T., Benedicto, A., Garcia-Gutiérrez, M., Alonso, U., 2014. Modeling cesium retention onto Na-, K- and Ca-smectite : Effects of ionic strength, exchange and competing cations on the determination of selectivity coefficients. Geochim. Cosmochim. Acta 128, 266–277. http://dx.doi.org/10.1016/j.gca.2013.10.007

Motellier, S., Ly, J., Gorgeon, L., Charles, Y., Hainos, D., Meier, P., Page, J., 2003. Modelling of the ion-exchange properties and indirect determination of the interstitial water composition of an argillaceous rock. Application to the Callovo-Oxfordian low-water-content formation. Appl. Geochem. 18, 1517–1530. https://doi.org/10.1016/S0883-2927(03)00049-0

Nolin, D., 1997. Rétention de radioéléments à vie longue par des matériaux argileux. Influence d'anions contenus dans les eaux naturelles. Thesis, Univ. Paris 6, France, 1–219.

Palagyi, S., Stamberg, K., 2010. Transport of $^{125}I^-$, $^{137}Cs^+$, $^{85}Sr^{2+}$ in granitic rock and soil columns. J Radioanal. Nucl. Chem. 286, 309–316. https://doi.org/10.1007/s10967-010-0719-x

Parkhurst, D.L., Appelo, C.A., 1999. User's Guide to PHREEQC (Version 2)—A computer program for speciation, batch-reaction, one-dimensional transport, and inverse geochemical calculations. United States Geological Survey, Water Resources Investigations Report 99-4259, Washington DC.

Peynet, V., 2003. Rétention d'actinide et de produits de fission par des phases solides polyminérales. Thesis, Univ. Paris 6, France, 1–256.

Poinssot, C., Baeyens, B., Bradbury, M. H., 1999. Experimental and modelling studies of caesium sorption on illite. Geochim. Cosmochim. Acta, 63, 3217–3227.

Porro, I., Newman, M.E., Dunnivant, F.M., 2000. Comparison of batch and column methods for determining strontium distribution coefficients for unsaturated transport in basalt. Environ. Sci. Technol., 34 (9), 1679-1686.

Rafferty, P., Shiao, S. Y., Binz, C. M., Meyer, R. E., 1981. Adsorption of Sr(II) on clay minerals: Effects of salt concentration, loading and pH. J. Inorg. Nucl. Chem.43, 797–806. https://doi.org/10.1016/0022-1902(81)80224-2

Reinholdt, M.X., Hubert, F., Faurel, M., Tertre, E., Razafitianamaharavo, A., Francius, G., Prêt, D., Petit, S., Béré, E., Pelletier, M., Ferrage, E., 2013. Morphological properties of vermiculite particles in size-selected fractions obtained by sonication. Appl. Clay Sci. 77–78, 18-32. https://doi.org/10.1016/j.clay.2013.03.013

Reinoso-Maset, E., Ly, J., 2014. Study of major ions sorption equilibria to characterize the ion exchange properties of kaolinite. J. Chem. Eng. Data, 59 (12), 4000-4009. https://doi.org/10.1021/je5005438

Reynolds, R.C., 1985. Description of program NEWMOD© for the calculation of the one-dimensional X-ray diffraction patterns of mixed-layered clays. User Manual; R.C. Reynolds Ed., 8 Brook Road, Hanower, New Hampshire, 03755.

Samadfam M., Jintoku T., Sato S., 2000. Effect of humic acid on the sorption of Sr(II) on kaolinite. J. Nucl. Sci. Technol. 37, 180-185. http://doi.org/10.1080/18811248.2000.9714882.

Savoye, S.; Beaucaire, C.; Fayette, A.; Herbette, M.; Coelho, D., 2012. Mobility of cesium through the callovo-oxfordian clay stones under partially saturated conditions. Environ. Sci. Technol. 46 (5), 2633–2641. https://doi.org/10.1021/es2037433 |

Sawhney, B.L., 1972. Selective sorption and fixation of cations by clay minerals. Clay Clay Min. 20, 93-100.

Schweich, D., Sardin, M., 1981. Adsorption, partition, ion exchange and chemical reaction in batch reactors or in column—a review. J. Hydrol. 50, 1– 33.

Simunek, J., van Genuchten, M.Th.,Sejna, M., 2008. The HYDRUS-1D software package for simulating the one-dimensional movement of water, heat, and multiple solutes in variably saturated media. Version 4.0. HYDRUS Software Ser. 3. Dep.of Environmental Sciences, Univ. Of California, Riverside.

Siroux, B., Beaucaire, C., Tabarant, M., Benedetti, M. F., Reiller, P. E. 2017. Adsorption of strontium and caesium onto an Na-MX80 bentonite: Experiments and building of a coherent thermodynamic modelling. Appl. Geochem. 87, 167–175. http://dx.doi.org/10.1016/j.apgeochem.2017.10.022

Siroux, B., Wissocq, A., Beaucaire, C., Latrille, C., Petcut, C., Calvaire, J., Tabarant, M., Benedetti, M. F., Reiller, P. E. 2018. Adsorption of strontium and caesium onto an Na-illite and Na-illite/Na-smectite mixtures: Implementation and application of a multi-site ion-exchange model. Appl. Geochem. 99, 167–175. https://doi.org/10.1016/j.apgeochem.2018.10.024

Steefel, C.I., Caroll, S., Zhao, P., Roberts, S., 2003. Cesium migration in Hanford sediment: a multisite cation exchange model based on laboratory transport experiments. J. Contam. Hydrol. 67, 219–246. https://doi.org/10.1016/S0169-7722(03)00033-0

Szenknect, S., Ardois, C., Gaudet, J.P., Barthes, V., 2005. Reactive transport of 85Sr in a Chernobyl sand column: static and dynamic experiments and modeling. J. Contam. Hydrol. 76, 139–165. https://doi.org/10.1016/j.jconhyd.2004.08.003

Szenknect, S., Ardois, C., Dewière, L., Gaudet, J.P., 2008. Effects of water content on reactive transport of 85Sr in Chernobyl sand columns. J. Contam. Hydrol. 100, 47-57. https://doi.org/10.1016/j.jconhyd.2008.05.004

Tertre, E., Beaucaire, C., Coreau, C., Juery, A., 2009. Modelling Zn(II) sorption onto clayey sediments using a multi-site ion-exchange model. Appl. Geochem. 24, 1852–1861. https://doi.org/10.1016/j.apgeochem.2009.06.006

Tertre, E., Hubert, F., Bruzac, S., Pacreau, M., Ferrage, E., Prêt, D., 2013. Ion-exchange reactions on clay minerals coupled with advection/dispersion processes. Application to Na^+/Ca^{2+} exchange on vermiculite: Reactive-transport modeling, batch and stirred flow-through reactor experiments. Geochim. Cosmochim. Acta 112, 1-19. https://doi.org/10.1016/j.gca.2013.02.028

Tournassat, C., Grangeon, S., Leroy, P., Giffaut, E., 2013. Modeling specific pH dependent sorption of divalent metals on montmorillonite surfaces. A review of pitfalls, recent achievements and current challenges. Am. J. Sci., 313, 395–451. https://doi.org/10.2475/05.2013.01

Valocchi, A.J., Roberts, P.V., Parks, G.A. and Street, R.L. 1981a. Simulation of the transport of ion exchanging solutes using laboratory-determined chemical parameter values. Ground Water 19, 600-607.

Valocchi, A.J., Street, R.L. and Roberts, P.V., 1981b. Transport of ion-exchanging solutes in groundwater: Chromatographic theory and field simulation. Water Resources Res. 17, 1517-1527.

Villalobos, M., Leckie, J.O., 2000. Carbonate adsorption on goethite under closed and open CO_2 conditions. Geochim. Cosmochim. Acta, 64(22), 3787-3802.

Voegelin, A., Vulava, V.M., Huhnen, F., Kretzschmar, R., 2000. Multicomponent transport of major cations predicted from binary adsorption experiments. J. Contam. Hydrol. 46, 319–338.

Vulava, V.M., Kretzschmar, R., Rusch, U., Grolimund, D., Westall, J., Borkovec, M., 2000. Cation competition in a natural subsurface material: modelling of sorption equilibria. Environ. Sci. Technol. 34, 2149–2155.

Vulava, V.M., Kretzschmar, R., Barmettler, K., Voegelin, A., 2002. Cation competition in a natural subsurface material: prediction of transport behavior. Water Resour. Res. 38, 7-1-7-7. https://doi.org/10.1029/2001WR000262

Wahlberg, J.S., Baker, J.H., Vernon, R.W., Dewar, R.S., 1965. Exchange adsorption of strontium on clay minerals. U.S. Geol. Surv. Bull. 1140-C.

Wissocq, A., Beaucaire, C., Latrille, C., 2017. Ca and Sr sorption on Ca-illite: experimental study and modelling. Procedia Earth and Planetary Science 17, 662-665. https://doi.org/10.1016/j.proeps.2016.12.177

Wissocq, A., Beaucaire, C., Latrille, C., 2018. Application of the multi-site ion exchanger model to the sorption of Sr and Cs on natural clayey sandstone. Appl. Geochem. 93, 167–177. https://doi.org/10.1016/j.apgeochem.2017.12.010